

## SUPPLEMENTARY INFORMATION

### **Highly selective detection of an organophosphorus pesticide, methyl parathion, using Ag-ZnO-SWCNT based field-effect transistors**

T.H. Vignesh Kumar,<sup>a</sup> Suresh Kumar Raman Pillai,<sup>b</sup> Mary B. Chan-Park,<sup>b</sup> and Ashok K.

Sundramoorthy,<sup>\*,a</sup>

<sup>a</sup>Department of Chemistry, SRM Institute of Science and Technology, Kattankulathur-603 203,

Tamil Nadu, India

<sup>b</sup>School of Chemical and Biomedical Engineering, Nanyang Technological University, 62

Nanyang Drive, Singapore 637 459, Singapore

\*Corresponding author:

Ph: +91-44-27417686

Email: [ashokkus@srmist.edu.in](mailto:ashokkus@srmist.edu.in) ; [ashok.sundramoorthy@gmail.com](mailto:ashok.sundramoorthy@gmail.com)

## **1. Micro-fabrication of FETs**

The micro-fabrication of field effect transistors (FETs) was carried out in a class 1000 clean room at a controlled and dust-free environment to avoid contamination of FETs, which were fabricated on a p-type silicon (si) wafer (diameter: 7.62 cm, thickness: 375  $\mu\text{m}$ , polished: single side, orientation:  $\langle 100 \rangle$ , resistivity: 1-10  $\Omega\text{ cm}$ ). **Supplementary Scheme S1** shows the order of process and FET architecture. The P type Si wafer was cleaned by Radio Corporation of America (RCA) solutions. At first, we cleaned by RCA 1 solution ( $\text{NH}_4\text{OH}:\text{H}_2\text{O}_2:\text{H}_2\text{O}$  in 1:1:5, v/v) at 75° C for 10 min, and followed by RCA 2 solution ( $\text{HCl}:\text{H}_2\text{O}_2:\text{H}_2\text{O}$  in 1:1:6, v/v) at 75° C for 10 min. Finally, cleaned by RCA 3 solution ( $\text{HF}:\text{H}_2\text{O}$  in 1:50, v/v) at 25°C for 30 sec, rinsed thoroughly with distilled water, and dried under nitrogen (**Flow 1, Scheme S1 A**).<sup>1,2</sup> The cleaned Si wafer was passivated with 500 nm of  $\text{SiO}_2$  as gate dielectric layer by low pressure chemical vapour deposition (LP-CVD)/pyrogenic oxidation technique (First nano-oxidation & diffusion furnace, ET 6000) at 1100°C in atmosphere using a three-step dry (10 min) – wet (45 min) – dry (30 min) process (**Fig. S1**). This ensured rapid oxidation with a resultant low-stress  $\text{SiO}_2$  and a clean  $\text{SiO}_2/\text{Si}$  interface (**Flow 2, Scheme S1 A**). After  $\text{SiO}_2$  deposition on 3 inch Si substrate, thickness was measured by Ellipsometry solution (EC-400, J.A. Woollam Co. Inc). Five-point, fixed-angle (70°) Ellipsometry indicated that the top  $\text{SiO}_2$  thicknesses were approximately 550 to 580 nm (**Fig. S2 A & B & Table S1**). After this, 1.4  $\mu\text{m}$  layer of a photosensitive polymer (positive photoresist, AZ5214E) coated by spin coating (WS-650 MZ-23 NPP) (**Flow 3, Scheme S1A**). The photoresist becomes removable by ultraviolet light due to the splitting of chemical bonds and the structures with the resist mask are thus patterned, while the remaining photoresist was removed.<sup>1,3</sup> The lithography process was used to design the geometric pattern (photomask) to define the source and drain metal contacts using Heidelberg instrument. Finally, light treated wafer was immersed in AZ351B

developer for 25 sec to remove the unwanted photoresist from the wafer (**Flow 4, Scheme S1 A**). Then, thin layers of titanium (Ti, thickness of 12 nm) and platinum (Pt, thickness of 220 nm) were deposited on mask patterned photoresist through physical vapour deposition by sputtering (Techport sputter coater-1) (**Flow 5, Scheme S1 A**) method.<sup>3</sup> Followed by lift-off in acetone and isopropanol were used to reveal the source and drain electrodes (**Flow 6, Scheme S1 A**).<sup>4-6</sup> After this, Ti/Pt electrode thickness was measured by Dektakxt (Bruker) instrument. The results indicated that the source and drain (Ti/Pt) electrodes thicknesses were approximately 260 to 265 nm (**Fig. S3**). Finally, dice the wafer into smaller dies  $1.6\text{ cm} \times 1.6\text{ cm}$  using disco automatic dicing saw instrument (DAD 322, diamond blade, 22000 RPM) as shown in **Scheme S1 B and C**. In total 20 devices were prepared by this method.

## **2. Experimental setup for electrical measurements**

s-SWCNT-FETs were fabricated by drop-casting the s-SWCNTs dispersion onto silica substrates with pre-deposited Ti/Pt electrodes (as shown in **Scheme S1 and Fig. S4**). The experimental setup for electrical measurements is shown in **Fig. S7**. The fabricated FET sensor devices were placed in a probe station connected with oil free dry vacuum pump, with its tungsten electrodes (diameter: 0.2 mm) connected to a semiconductor parameter analyser. The resistance of the s-SWCNTs/FET devices are  $\sim 8\text{-}9\text{ M}\Omega$ .<sup>7</sup>





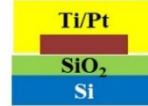

## **3. Full sweep transfer characteristics**

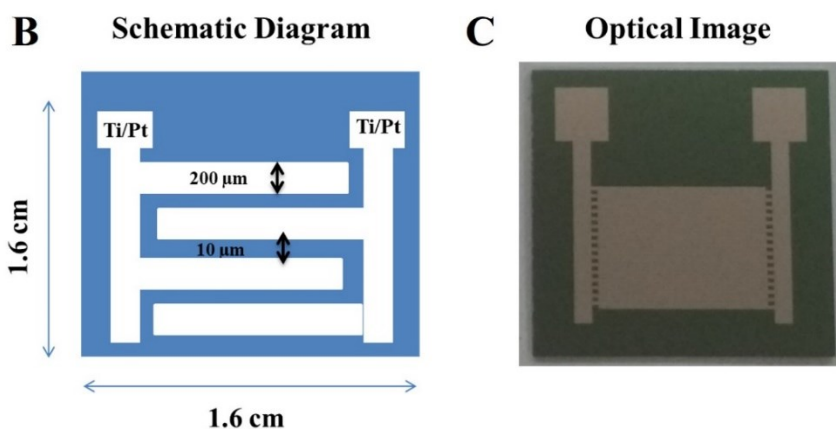
The forward and backward sweep of s-SWCNTs/FET transfer characteristics ( $I_{\text{DS}} - V_{\text{GS}}$ ) are displayed in **Fig. S8 (A)**, where the forward sweep corresponds to the same s-SWCNTs/FET measured data displayed in **Fig. 5B**. The FET illustrates hysteresis, the origin of which has early been attributed to adsorbed oxygen and water molecules.<sup>8</sup> Recent studies has shown that hysteresis can be subtracted from s-SWCNT/FETs via functionalization.<sup>9</sup> The forward sweep measured data presented in the main text.<sup>10</sup> **Fig. S8 (B)** illustrates the histogram of on/off ratios for s-SWCNT/FET

devices prepared from obtained s-SWCNTs solution. The drain to source current as well as the drain to gate leakage current was recorded for s-SWCNTs/FET (**Fig. S8 (C&D)**).

## SUPPLEMENTARY FIGURES

**A**

Flow	Bay	Process	Device Cross Section
1	Wet etch	RCA	
2	Diffusion	Pyrogenic Oxidation / LP CVD	
3	Lithography	Optical Lithography	
4	Lithography	Mask writing	
5	Films	Metal Deposition Ti/Pt (12 nm/220 nm)	
6	Lift off	Metal Lift off	



**Scheme. S1.** FET fabrication process flow. (A) Fabrication by stepwise process, (1) Si substrate cleaning process, (2) SiO<sub>2</sub> deposition, (3 & 4) Photomask and mask writing for metal deposition, (5) Metal deposition for source-drain contact and (6) Metal lift-off. (B) Schematic diagrams of device structure. (C) Optical image of device structure.

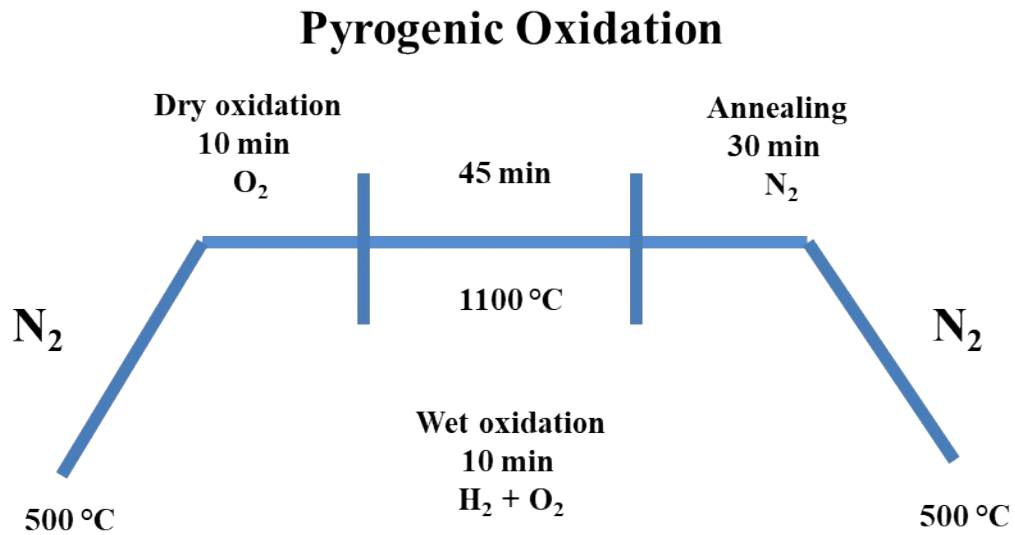


**Fig. S1.** 500 nm of silicon dioxide (SiO<sub>2</sub>) deposited on 3 inch Si wafer by low pressure chemical vapour deposition/pyrogenic oxidation. The schematic diagram depicts the preparatory process for the SiO<sub>2</sub> deposition.

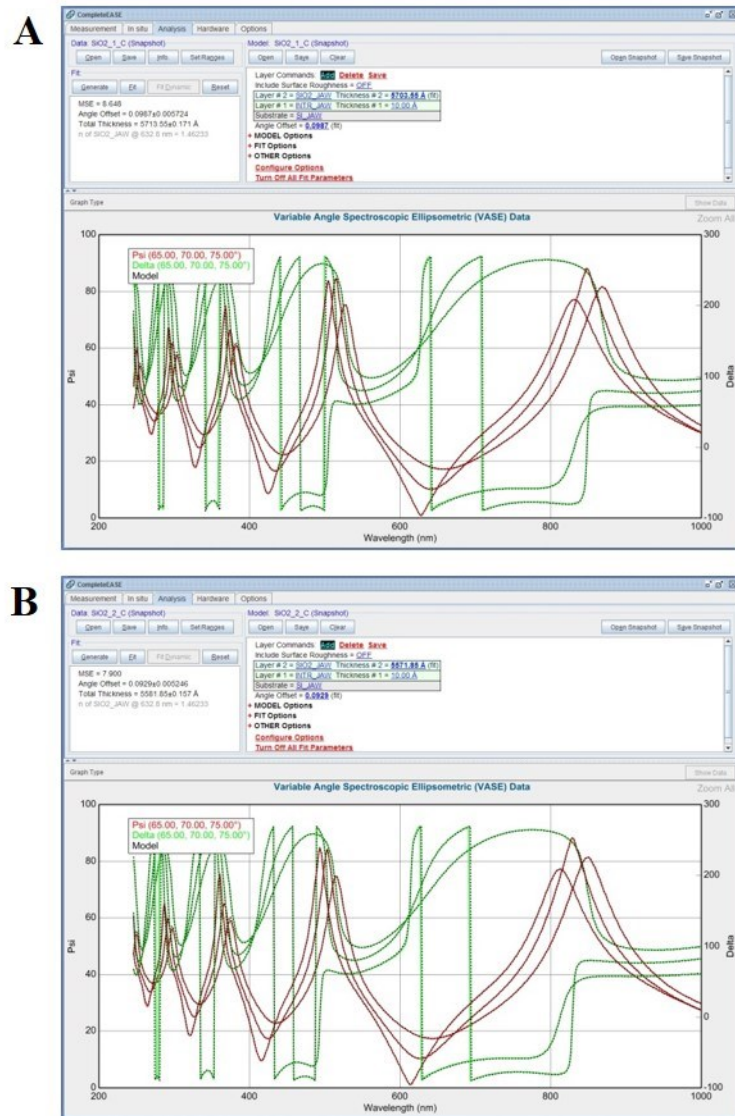


**Fig. S2.** SiO<sub>2</sub> thickness was measured on 3 inch Si wafer by Ellipsometry (EC-400, J.A. Woollam Co. Inc). **(A)** Sample A- SiO<sub>2</sub> thickness value is 570.36 nm (center place). **(B)** Sample B- SiO<sub>2</sub> thickness value is 557.18 nm (center place). Measured thickness on both samples at different places were also indicated in **Table S1**. Refractive index for both samples was 1.46.

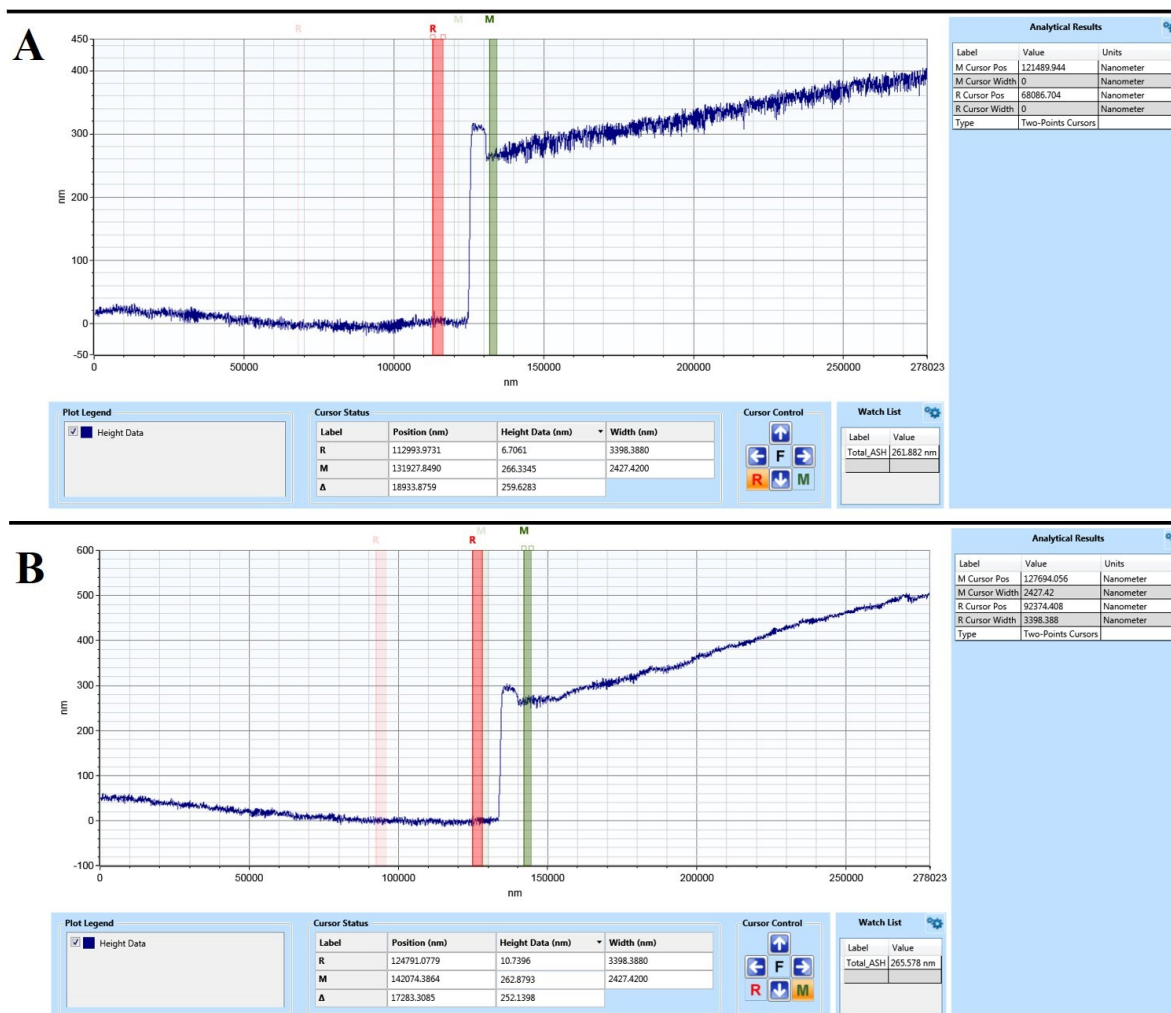


**Fig. S3.** Source and drain electrode (Ti/Pt) thicknesses were measured by Dektakxt (Bruker). **(A)** Sample A - Ti/Pt thickness value was 261.88 nm. **(B)** Sample B - Ti/Pt thickness value was 265.57 nm.



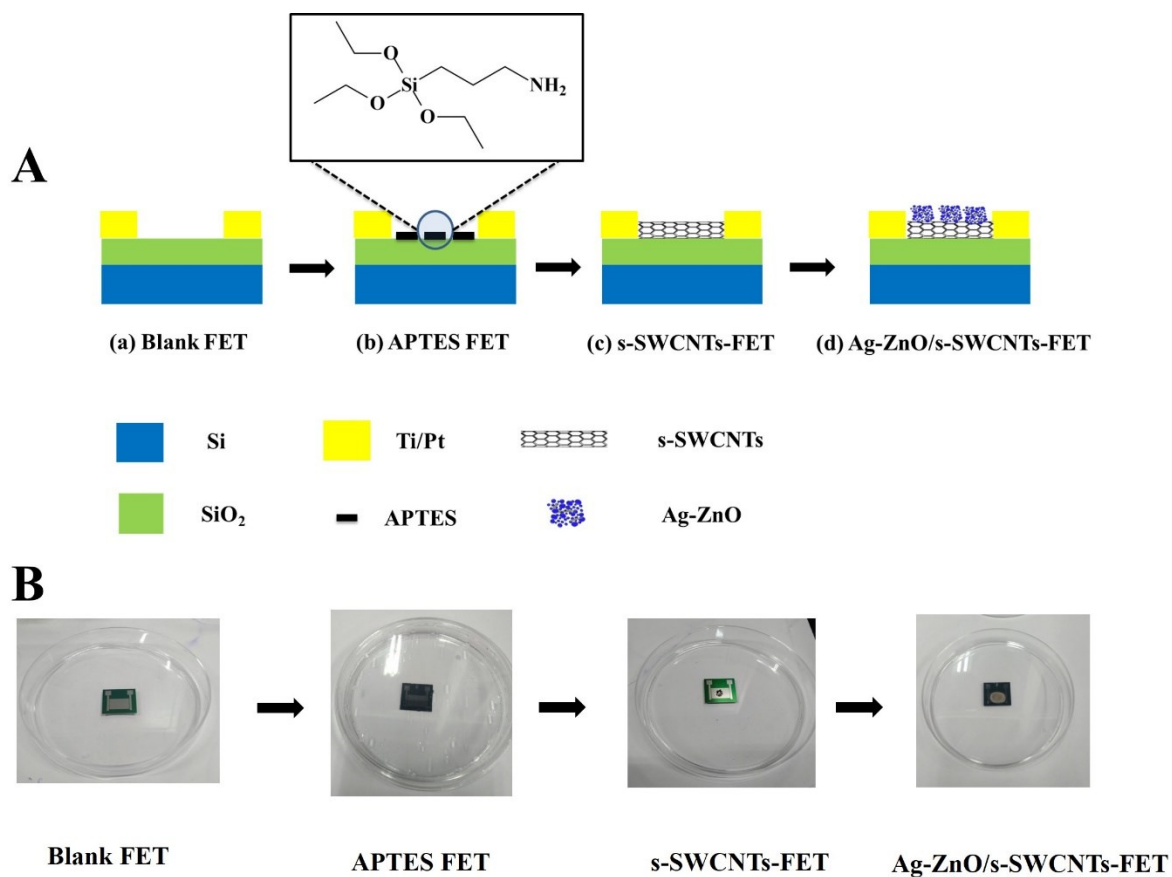


**Fig. S4 (A&B).** Schematic and photographic images were depicting preparatory process for the Ag-ZnO/s-SWCNTs-FET based non-enzymatic MP sensor. This sensor can selectively respond to MP.

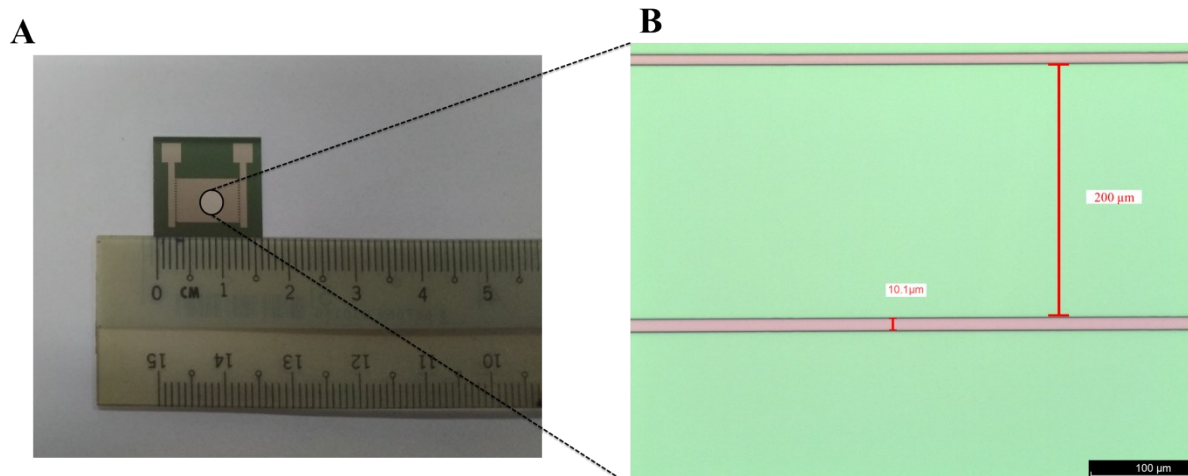


**Fig. S5.** (A) Optical images of blank FET device with a scale. (B) Fabricated device channel width and channel length were measured by microscope.

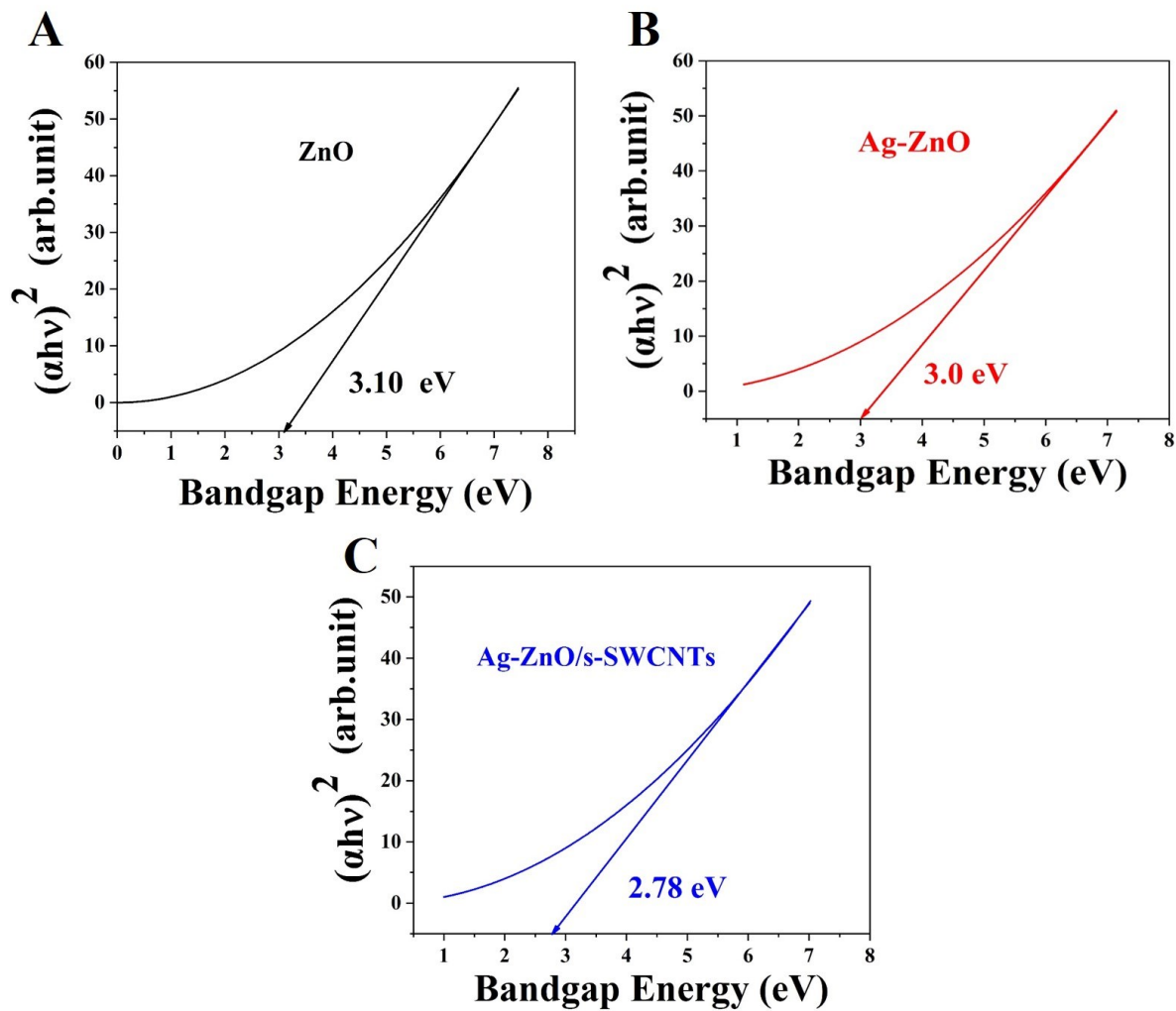


**Fig. S6.** Tau plots for band gap energy analysis: (A) Pure ZnO, (B) Ag-ZnO and (C) Ag-ZnO/s-SWCNTs

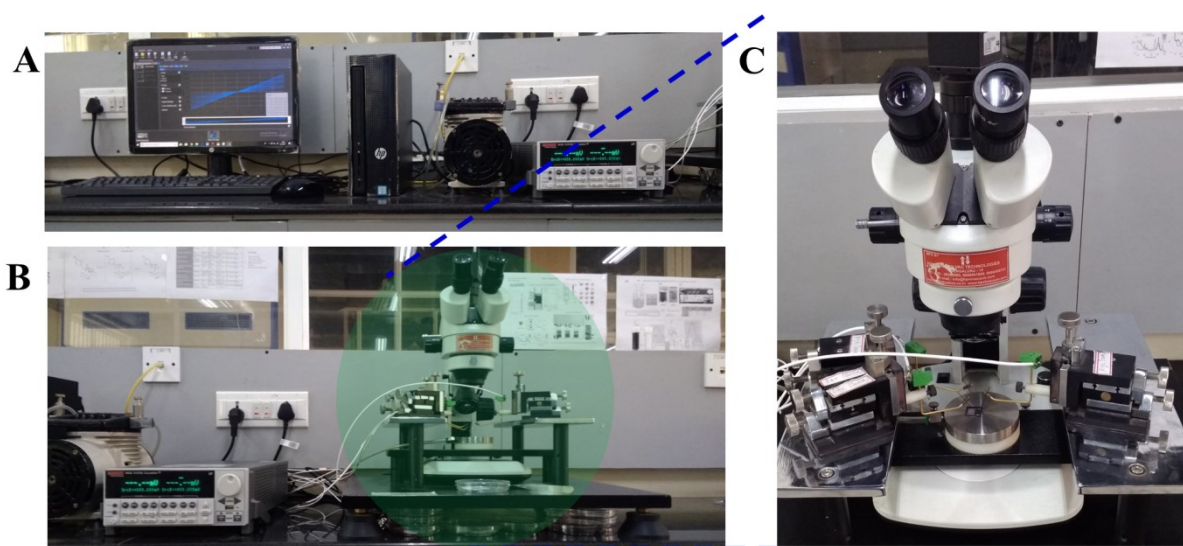


**Fig. S7.** Photographic images of experimental setup for FET sensing measurements. (A) Electrical measurements were performed by Keithley semiconductor parameter analyser, model 2612B connected with hp computer. Kickstart software was used for the FET sensing measurements. (B) Keithley semiconductor parameter analyser connected with the probe station. (C) Complete view of probe station.

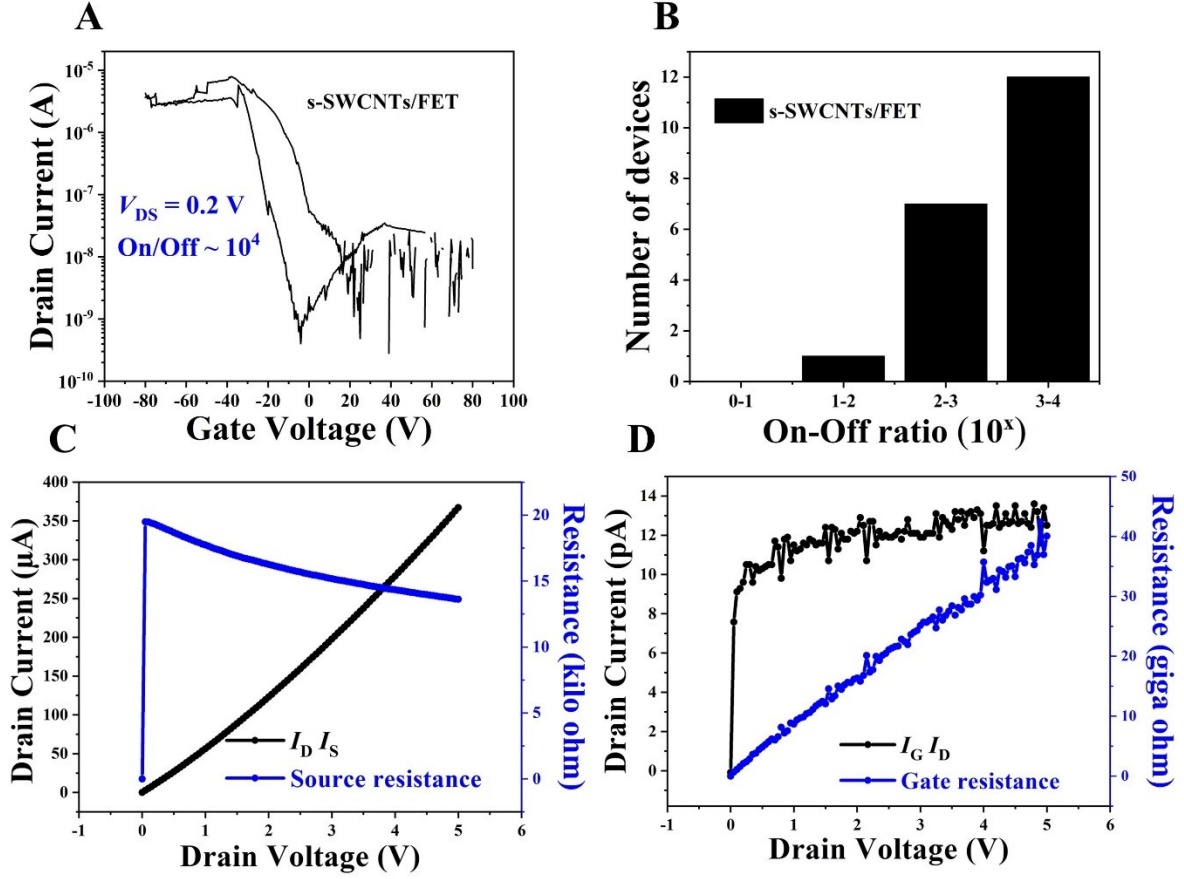


**Fig. S8** (A). Typical transfer characteristics of s-SWCNTs/FET device at  $V_{DS} = 0.2 \text{ V}$ . (B) Histogram of on/off ratios for fabricated s-SWCNTs/FET devices. The number x in the x-axis represent  $10^x$ . (C) Drain to source current and (D) drain to gate leakage current of s-SWCNTs/FET device. The voltage was swept from 0 to 5 V.

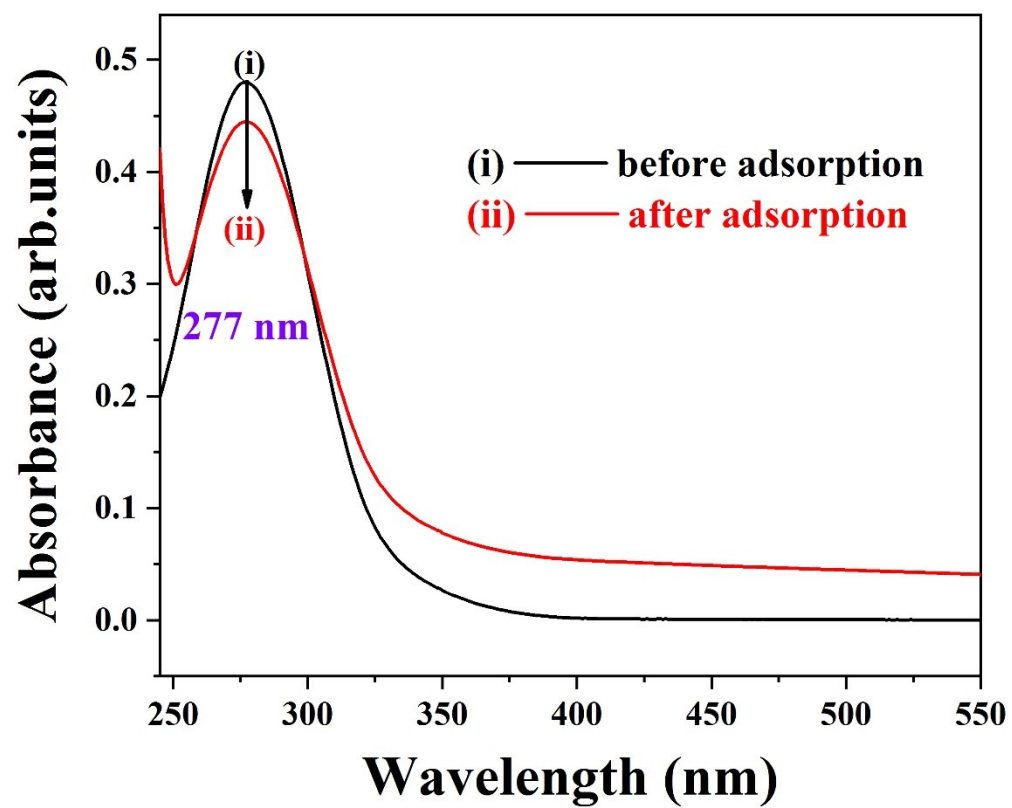


**Fig. S9.** UV-Visible spectra of MP (i) before and (ii) after treatment with Ag-ZnO.

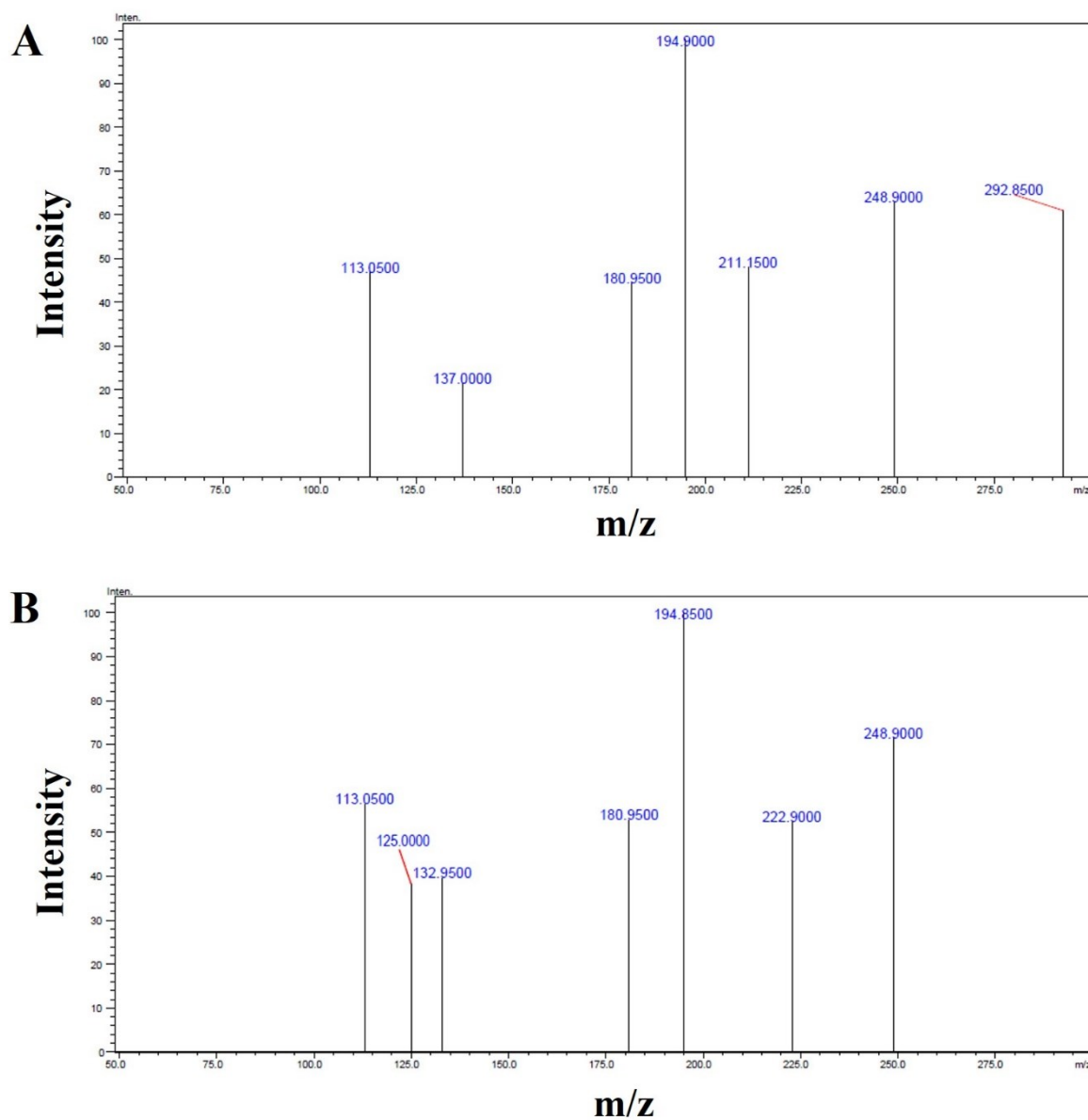


**Fig. S10.** LC-MS spectra of MP (A) (control) and (B) after treated with Ag-ZnO/s-SWCNTs composite.

**A**

**B**



**Fig. S11. (A &B)** Photographic images of rice and soil sample spiked with MP.



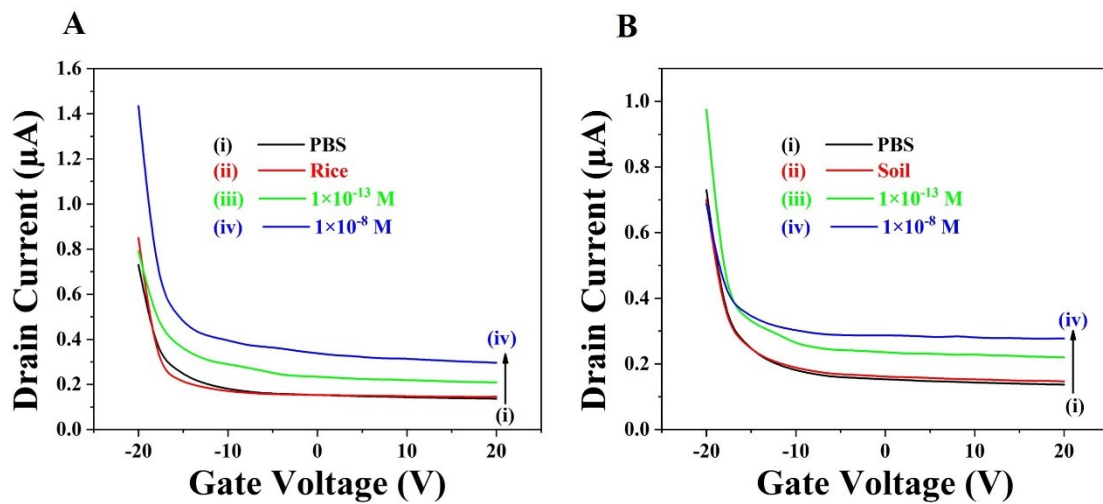


**Fig. S12.** (A & B)  $I_{\text{DS}}-V_{\text{GS}}$  transfer curve of Ag-ZnO/s-SWCNTs-FET, before (blank) and after adding 10  $\mu\text{L}$  of two different rice and soil spiked with MP concentrations (0,  $1 \times 10^{-13}$  M and  $1 \times 10^{-8}$  M) in 0.1 M PBS (pH 2).

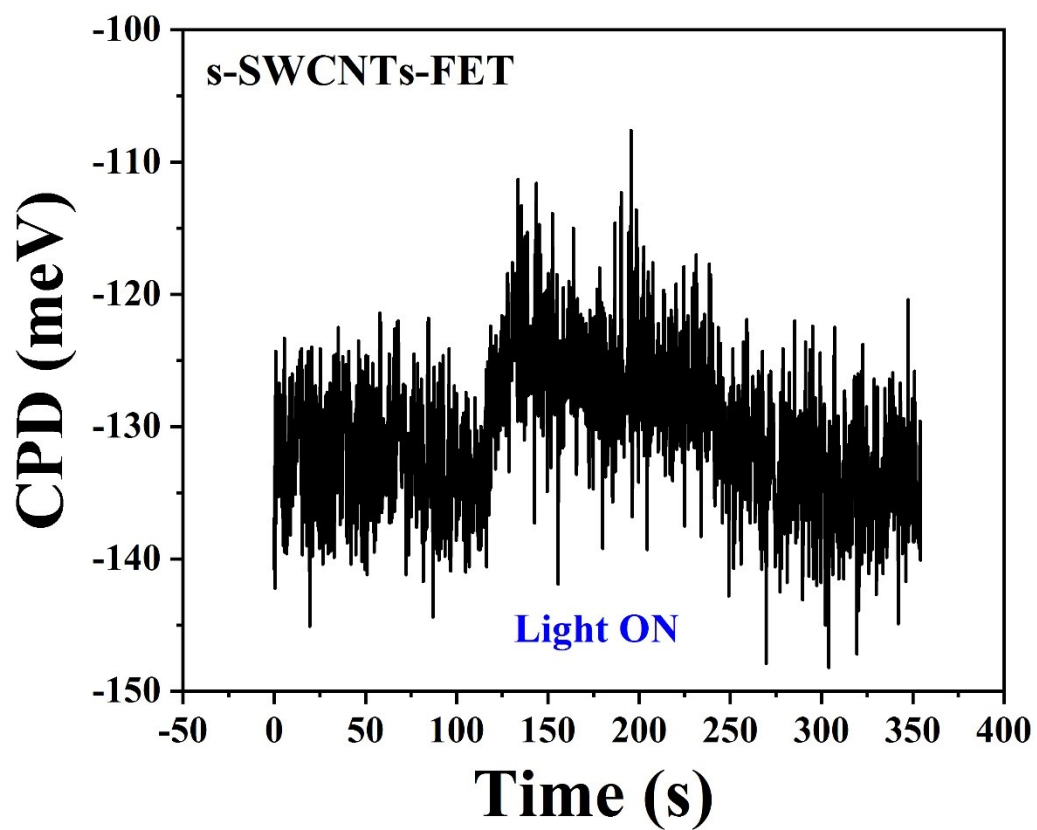


**Fig. S13.** The dynamic response and recovery curve of s-SWCNTs sensor to visible light is recorded by illuminating 70 mW/cm<sup>2</sup> QTH source.

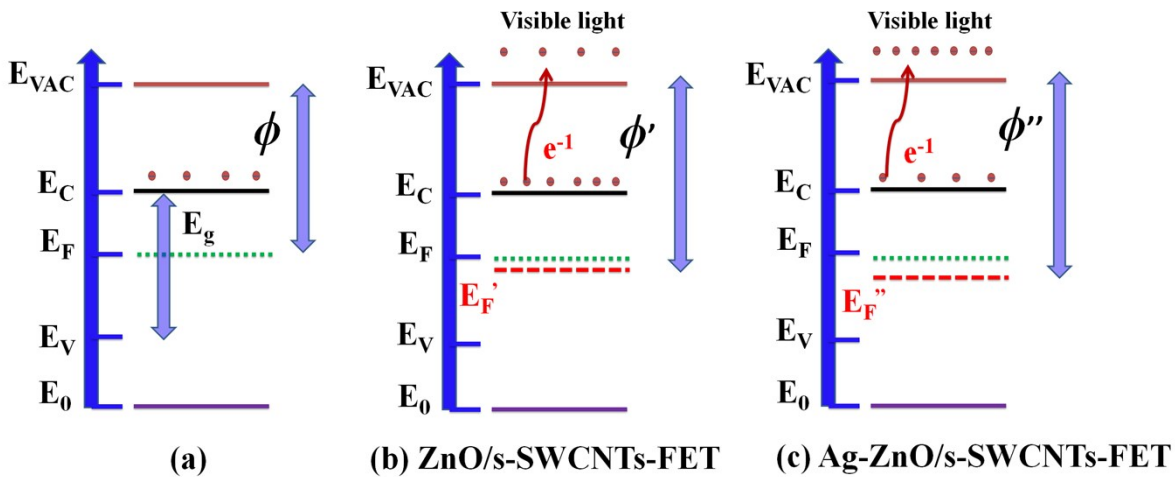


**Fig. S14.** (a) Energy band diagram for the semiconductor, (b & c) increase in  $E_F$  level upon addition of electron donating ZnO and Ag-ZnO.

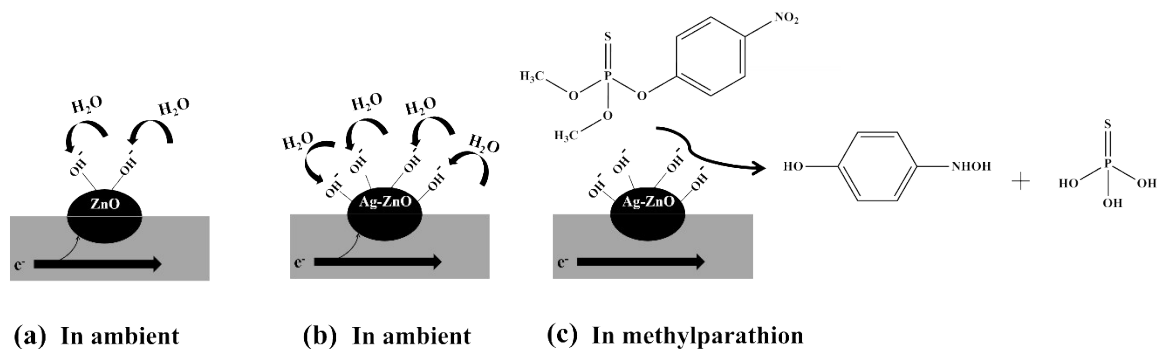


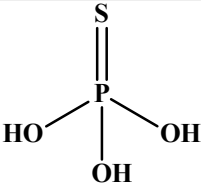
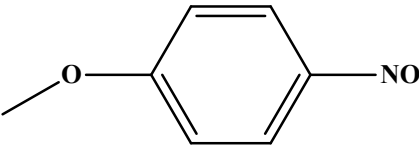
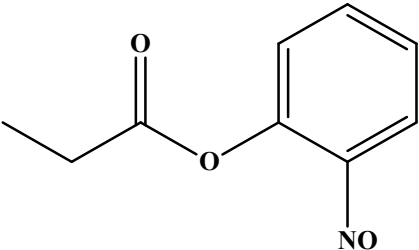
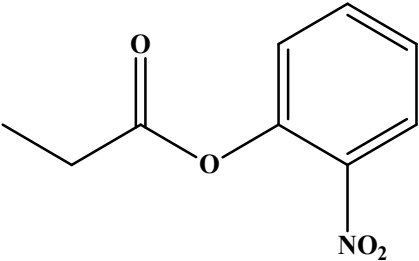
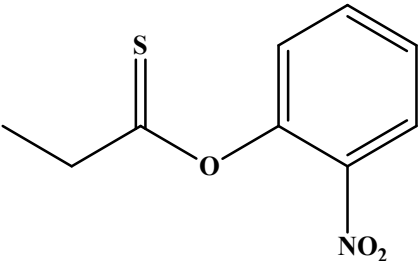
**Fig. S15.** Schematic representation of the ZnO and Ag-ZnO composite based MP sensing process.

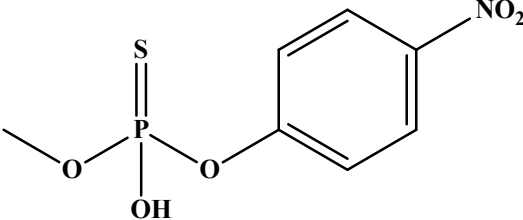
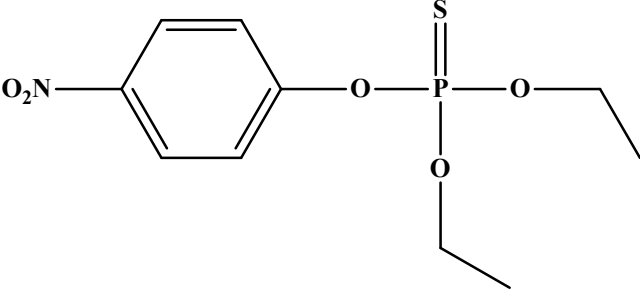
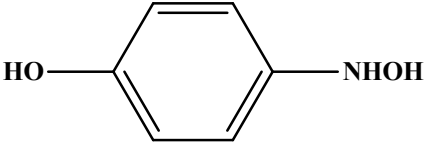
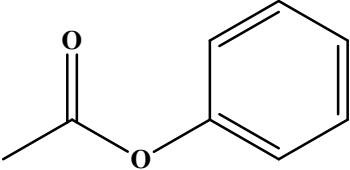
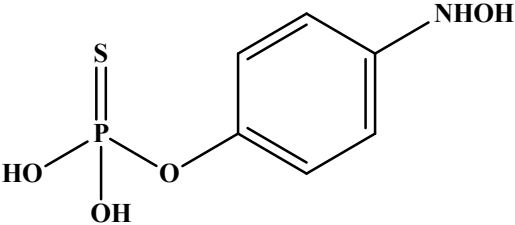
## SUPPLEMENTARY TABLES

**Table S1.** Measured SiO<sub>2</sub> thickness values are listed here.

<b>Place of wafer</b>	<b>Sample A Thickness value (nm)</b>	<b>Sample B Thickness value (nm)</b>
<b>Center</b>	570.36	557.18
<b>Left</b>	572.83	562.34
<b>Right</b>	570.14	559.68
<b>Top</b>	563.71	555.42
<b>Down</b>	575.27	563.02

**Table S2. The hydrolysis products of MP identified by LC-MS spectrum.**

Compounds	Fragments (m/z)	Elemental Composition	Structures	Name
a	113.05	H <sub>3</sub> O <sub>3</sub> PS		Phosphorothioic O,O,O-acid
b	137.00	C <sub>7</sub> H <sub>7</sub> NO <sub>2</sub>		1-methoxy-4-nitrosobenzene
c	180.95	C <sub>9</sub> H <sub>9</sub> NO <sub>3</sub>		2-nitrosophenyl propionate
d	194.90/194.85	C <sub>9</sub> H <sub>9</sub> NO <sub>4</sub>		2-nitrophenyl propionate
e	211.15	C <sub>9</sub> H <sub>9</sub> NO <sub>3</sub> S		O-(2-nitrophenyl) propanethioate

f	248.90	C <sub>7</sub> H <sub>8</sub> NO <sub>5</sub> PS		O-methyl O-(4-nitrophenyl) O-hydrogen phosphorothioate
g	292.85	C <sub>10</sub> H <sub>14</sub> NO <sub>5</sub> PS		O,O-diethyl O-(4-nitrophenyl) phosphorothioate
h	125.00	C <sub>6</sub> H <sub>7</sub> NO <sub>2</sub>		4-(hydroxyamino) phenol
i	132.95	C <sub>8</sub> H <sub>8</sub> O <sub>2</sub>		Phenyl acetate
j	222.90	C <sub>6</sub> H <sub>8</sub> NO <sub>4</sub> PS		O-(4-(hydroxyamino) phenyl) O,O-dihydrogen phosphorothioate

**Table S3.** Analytical comparison of our non-enzymatic FET sensor performance against other reported sensors for MP.

Proposed electrode	Method	Technique	Linear range	Limit of detection (LOD)	References
AChE/SF/MWCNTs/GCE	Enzymatic	Amperometry	$3.5 \times 10^{-6}$ to $2 \times 10^{-3}$ M	$5 \times 10^{-7}$ M	11
Au/ssDNA-SWCNT/PANI-AChE/GCE	Enzymatic	SWV	$1 \times 10^{-11}$ to $1 \times 10^{-6}$ M	$1 \times 10^{-12}$ M	12
BSA/AChE-Glu-s-SWCNTs/GCE	Enzymatic	SWV	$1 \times 10^{-10}$ to $5 \times 10^{-6}$ M	$3.75 \times 10^{-11}$ M	13
NF/AChE-CS/NiO-CGR-NF/GCE	Enzymatic	Amperometry	$1 \times 10^{-13}$ to $1 \times 10^{-10}$ M; $1 \times 10^{-10}$ to $1 \times 10^{-8}$ M	$5 \times 10^{-14}$ M	14
TiO <sub>2</sub> /Graphene/GCE	Non-Enzymatic	LSV	$2.0 \times 10^{-9}$ to $5.0 \times 10^{-6}$ M $5.0 \times 10^{-6}$ to $1.0 \times 10^{-6}$ M	$1.0 \times 10^{-9}$ M	15
NPG/GCE	Non-Enzymatic	DPV	$0.5 \times 10^{-6}$ to $1.5 \times 10^{-4}$ M	$2.0 \times 10^{-8}$ M	16
Ag/GNRs/SPCE	Non-Enzymatic	Amperometry	$5 \times 10^{-9}$ to $2.78 \times 10^{-3}$ M	$0.5 \times 10^{-9}$ M	17
CP5-rGO/GCE	Non-Enzymatic	DPV	$1 \times 10^{-9}$ to $1.5 \times 10^{-4}$ M	$0.3 \times 10^{-9}$ M	18
Ag-ZnO/s-SWCNTs-FET	Non-Enzymatic	Electrical Transport ( $I_{DS}$ - $V_{GS}$ )	$1 \times 10^{-16}$ to $1 \times 10^{-4}$ M	$0.27 \times 10^{-16}$ M	This work

Acetylcholinesterase (AChE); silk fibroin (SF); multi walled carbon nanotubes (MWCNTs); glassy carbon electrode (GCE); gold (Au); single strand oligonucleotide (ssDNA); single walled carbon nanotube (SWCNT); polyaniline (PANI); square wave voltammetry (SWV); bovine serum albumin (BSA); glutaraldehyde (Glu); Nafion (NF); chitosan (CS); nickel oxide (NiO); carboxylic graphene (CGR); titanium dioxide (TiO<sub>2</sub>); linear sweep voltammetry (LSV); nanoporous gold (NPG); differential pulse voltammetry (DPV); silver (Ag); graphene nanoribbons (GNRs); screen printed carbon electrode (SPCE); pillar[5]arene (CP5); reduced graphene oxide (rGO).

**Table S4.** Determination of spiked MP in rice and soil samples using Ag-ZnO/s-SWCNTs-FET.

Samples	MP added	Total MP found	RSD % (n=3)	Recovery (%)
Rice Sample-1	$1 \times 10^{-13}$ M	$1.02 \times 10^{-13}$ M	3.56	99.48
Rice Sample-2	$1 \times 10^{-8}$ M	$1.01 \times 10^{-8}$ M	1.86	97.90
Soil Sample-3	$1 \times 10^{-13}$ M	$1.10 \times 10^{-13}$ M	2.18	101.54
Soil Sample-4	$1 \times 10^{-8}$ M	$0.94 \times 10^{-8}$ M	1.91	97.91

#### SUPPLEMENTARY REFERENCES

- 1 S. K. Raman Pillai and M. B. Chan-Park, *ACS Appl. Mater. Interfaces*, 2012, **4**, 7047–7054.
- 2 Y. Wang, S. K. R. Pillai and M. B. Chan-Park, *Small*, 2013, **9**, 2960–2969.
- 3 G. S. Kulkarni and Z. Zhong, *Journal Vis. Exp.*, 2013, e50438.
- 4 Q. Cao, S. Han, G. S. Tulevski, Y. Zhu, D. D. Lu and W. Haensch, *Nat. Nanotechnol.*, 2013, **8**, 180.
- 5 B. K. Sarker, S. Shekhar and S. I. Khondaker, *ACS Nano*, 2011, **5**, 6297–6305.
- 6 T. Chen, L. Wei, Z. Zhou, D. Shi, J. Wang, J. Zhao, Y. Yu, Y. Wang and Y. Zhang, *Nanoscale Res. Lett.*, 2012, **7**, 644.



- 7 A. K. Sundramoorthy, S. Mesgari, J. Wang, R. Kumar, M. A. Sk, S. H. Yeap, Q. Zhang, S. K. Sze, K. H. Lim and M. B. Chan-Park, *J. Am. Chem. Soc.*, 2013, **135**, 5569–5581.
- 8 J. S. Lee, S. Ryu, K. Yoo, I. S. Choi, W. S. Yun and J. Kim, *J. Phys. Chem. C*, 2007, **111**, 12504–12507.
- 9 T.-J. Ha, D. Kiriya, K. Chen and A. Javey, *ACS Appl. Mater. Interfaces*, 2014, **6**, 8441–8446.
- 10 A. D. Franklin, G. S. Tulevski, S.-J. Han, D. Shahrjerdi, Q. Cao, H.-Y. Chen, H.-S. P. Wong and W. Haensch, *ACS Nano*, 2012, **6**, 1109–1115.
- 11 R. Xue, T.-F. Kang, L.-P. Lu and S.-Y. Cheng, *Appl. Surf. Sci.*, 2012, **258**, 6040–6045.
- 12 S. Viswanathan, H. Radecka and J. Radecki, *Biosens. Bioelectron.*, 2009, **24**, 2772–2777.
- 13 T. H. V. Kumar and A. K. Sundramoorthy, *Anal. Chim. Acta*, 2019, **1074**, 131–141.
- 14 L. Yang, G. Wang, Y. Liu and M. Wang, *Talanta*, 2013, **113**, 135–141.
- 15 B. Song, W. Cao and Y. Wang, *Fullerenes, Nanotub. Carbon Nanostructures*, 2016, **24**, 435–440.
- 16 X. Gao, Y. Gao, C. Bian, H. Ma and H. Liu, *Electrochim. Acta*, 2019, **310**, 78–85.
- 17 M. Govindasamy, V. Mani, S.-M. Chen, T.-W. Chen and A. K. Sundramoorthy, *Sci. Rep.*, 2017, **7**, 46471.
- 18 X. Tan, Y. Liu, T. Zhang, S. Luo, X. Liu, H. Tian, Y. Yang and C. Chen, *RSC Adv.*, 2019, **9**, 345–353.